Diffusion coefficient of the Al-based melt in the microstructure simulation

L. X. LI[a,b,*], X. B. BU[a,b], L. Q. ZHANG[a,b], B. W. ZHU[a,b], R. XU[a,b], S. P. WANG[a,b]
[a]*State Key Laboratory of Advanced Design and Manufacturing for Vehicle Body , Hunan University, Changsha, Hunan 410082, China*
[b]*College of Mechanical and Vehicle Engineering, Hunan University, Changsha 410082*

Numerical simulation of solidification grain structure is an effective alternative means in the prediction and controlling of the microstructure of castings other than actual casting experiment. The liquid-phase diffusion coefficient was one of the most important factors in the microstructure simulation, and affected the grain morphology. The liquid-phase diffusion coefficient was usually assumed to a constant in a wide variety of alloys. In the present paper, the diffusion coefficients of Al-based melts were calculated by the Miedema model, Extended Miedema model and Eyring model in different temperatures. In addition, a cellular automaton-finite element method was used to predict the solidification structure of an Al-2%Cu alloy and Al-9.75%Si-2%Cu alloy. Comparing the simulation results with the diffusion constant, the simulated results with calculated diffusion coefficient were in accord with the experimental ones well, and could accurately reflect the grains distribution, proportion, size of equiaxed and columnar grains.

(Received July 21, 2012; accepted July 11, 2013)

Keywords: Miedema model, Eying model, Diffusion coefficient, Microstructure

1. Introduction

The grain structure is of great importance for controlling the quality and properties of final casting products in solidification process. Several models have been developed for the prediction of microstructure formation of casting [1-4]. Numerical simulation experiences the stage of semi-quantitative simulation, fixed-points nucleation and deterministic model to quantitative simulation, random nucleation, and stochastic model. Cellular automation (CA)-finite element (FE) models are well suited to track the development of a columnar dendritic front in an undercooled liquid at the scale of the casting [3-4].

Simulations can be widely accepted as realistic descriptions of the process, some uncertainties must be eliminated in the simulation. In the CAFE model, reliable thermodynamic databases of a vast multi-component alloys have not been constructed, some necessary parameters are usually assumed. The diffusion coefficient of a melt is frequently assumed to the constant of 1×10^{-9} m^2/s in a mass of numerical simulations. Because the diffusion coefficients are usually based on concentration and temperature in the liquid, this simplification brings enormous incertitudes on the qualitative results in solidication microstructure simulations, the primary impediment associated with the modeling of atomic mobilities of melts is the lack of reliable liquid diffusivity data due to experimental difficulties caused by convection in melts.

Miedema model has been widely used to calculate some thermal properties of binary alloys [5-9]. Yan et al [10] combined the Toop model and the Miedema model to calculate the formation energy for ternary alloy systems, but the agreement between experimental data and calculations was a few improvement. Ding et al [11] also combined the Miedema model and the Toop model, and calculated the diffusion coefficient of the Ni-based alloy in 1473K. Eyring model had a widely impact on the theory of liquid structure [12-13]. Eyring model could directly calculate the liquid-phase diffusion coefficient, but it didn't consider the interaction of alloy composition. The diffusion coefficient of Eyring model was only the self-diffusion coefficient, could not really show the diffusion behavior in multi-component alloys.

The Miedema model and Extended Miedema model could calculate the diffusivities and interaction coefficient of the melt, but the lack of reliable liquid diffusivity data were the major obstacle. The self-diffusion coefficient was a main parameter of liquid diffusivity, and it could be calculated with temperature by the Eyring model. The Extended Miedema model contained the relation of the self-diffusion coefficient and liquid diffusivity, and took interaction coefficient of multi-component alloys under advisement. So the self-diffusion coefficient data should be taken into the Extended Miedema model to modify the data.

In the work, the diffusion coefficient of an Al-2%Cu melt and Al-9.75Si-2%Cu melt were calculated with the theoretical method by the Miedema model, Extended Miedema model and Eyring model. The self-diffusion coefficient was calculated by the Eyring model; the

liquid-phase diffusion coefficient was calculated by the self-diffusion coefficient, Miedema model and Extended Miedema model. With the liquid-phase diffusion coefficient, a 3D microstructure was also accurately predicted based on the cellular automaton-finite element method.

2. Experiment

The experiment was carried out with preset ingots model of 40 mm and 60 mm diameter, and the model was height of 125 mm. The casting materials were the Al-2%Cu alloy and Al-9.75%Si-2%Cu alloy, respectively. The initial temperature of the mold was 170℃, and the pouring temperature was about 720℃ in the experiment. The shape of the mold was shown in Fig. 1. Asbestos was wrapped around mold to produce an insulation effect. The heat transfer of the upper mold was defined as air-cooling. The grains size of 40mm would be observed in Fig. 1. The numerical simulation was used by the ProCAST software. The nucleation parameters were shown in Table 1.

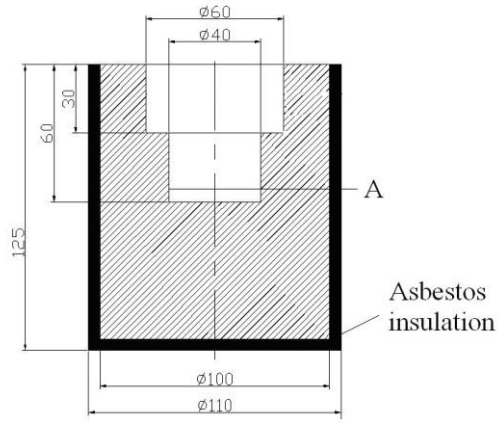

Fig. 1. Shape and dimensions of experimental casting mold (mm).

Table 1. Material properties and model parameters used in simulations.

Liquidus temperature, *T*/K (Al-2%Cu)	929
Liquidus temperature, *T*/K (Al-9.75%Si-2%)	864
Liquidus slope, *m*/K/wt.% (Al-2%Cu)	-0.98
Liquidus slope, *m*/K/wt.% (Al-9.75%Si-2%)	-6.5
Gibbs-Thompson coefficient, Γ	1×10^{-7}
maximum nucleation densities, n_{max}/m^3	1×10^{7}
mean undercooling, $\triangle T_N$/K	0.5
Standard deviation, $\triangle T_\sigma$/K	0.1

3. Calculation model

3.1 Eyring model

The self-diffusion coefficient was far from integrity with variational temperature in different alloys. Eyring model could calculate the diffusion coefficient of the liquid in different temperature, but it didn't consider the interaction coefficient and the activity coefficient in the alloy. So the diffusion coefficient of the liquid could be only used as the self-diffusion coefficient (D_i^*) in the Eyring model.

$$D_{ij} = \frac{kT}{\xi_i u_j}\left(\frac{\lambda_{1j}}{\lambda_{2j}\lambda_{3j}}\right)^{1/3}\frac{F_{jj}F_{ij}^{'}}{F_{jj}^{'}F_{ij}}\exp\left(\frac{E_{u,j}-E_{D,ij}}{RT}\right) \quad (1)$$

$$\lambda_{1j} = \lambda_{2j} = \lambda_{3j} = (v_j / N)^{1/3} \quad (2)$$

Where D_{ij} was the diffusion coefficient, T was the experimental temperature, u_j was the viscosity of the solvent, λ_{1j}, λ_{2j}, λ_{3j} were the distance between the molecules of the three coordinate directions, respectively. V_j was the molar volume of solvent, N was the Avogadro constant, $E_{u,j}$ and $E_{D,ij}$ were the activation energy and diffusion activation energy, respectively. ξ_i was the geometric parameters of the number molecules around solute molecules.

$$\xi_i = 6\left(\frac{V_i}{V_j}\right)^{1/6} \quad (3)$$

$$\frac{F_{jj}F_{ij}^{'}}{F_{jj}^{'}F_{ij}} = \left(\frac{m_j}{m_i}\right)^{1/2}\left(\frac{\rho_i}{\rho_j}\right)^{1/3} = \left(\frac{M_j}{M_i}\right)^{1/6}\left(\frac{V_j}{V_i}\right)^{1/3} \quad (4)$$

$F_{ij}^{'}$ was the diffused partition function of activated state. F_{ij} was the diffused partition function of molecular equilibrium. $F_{jj}^{'}$ was the viscosity partition function of activated state. F_{jj} was the viscosity partition function of molecular equilibrium. m was the molecular weight.

$$D_{ij} = \frac{kT}{\xi_i u_j}\left(\frac{N}{V_j}\right)^{1/3}\left(\frac{M_j}{M_i}\right)^{1/6}\left(\frac{V_j}{V_i}\right)^{1/3}\exp\left[\frac{\frac{E_{u,j}}{2}-\left(\frac{E_{u,j}}{2}\right)^{\frac{\xi_i}{\xi_i+1}}\left(\frac{E_{u,i}}{2}\right)^{\frac{1}{\xi_i+1}}}{RT}\right] \quad (5)$$

When calculating the self-diffusion in the ternary alloy, the symbol *i* was replaced by solute composition, the symbol j was replaced by solvent composition.

3.2 Viscosity in Eyring mode

The alloy viscosity was changed with the temperature. In this paper, the simulation was adopted the solution viscosity of the melt. This viscosity was provided by ProCAST in Fig. 2.

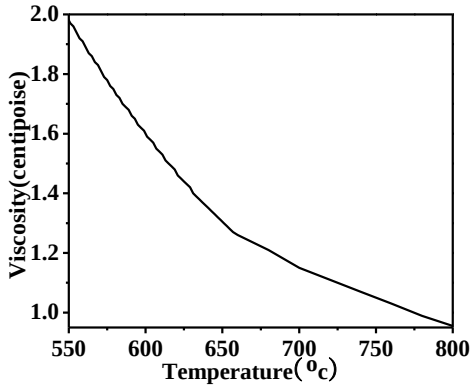

(a)

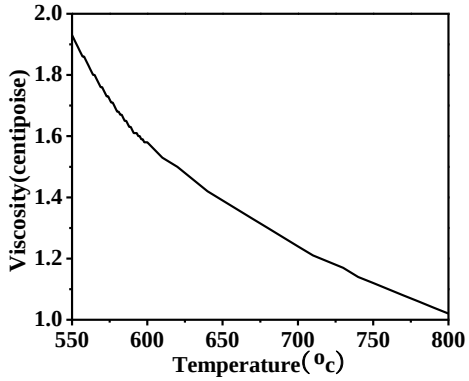

(b)

Fig. 2. Variation of viscosity with temperature (a) Al-2%Cu alloy (b) Al-9.75Si-2%Cu alloy.

3.3 Miedema model

According to Miedema model [11], the formation energy ΔH_{ij} of the $i-j$ alloys could be calculated as follow

$$\Delta H_{ij} = f_{ij}\frac{x_i[1+u_i x_j(\varphi_i-\varphi_j)x_j[1+u_j x_i(\varphi_j-\varphi_i)]]}{x_i[1+u_i x_j(\varphi_i-\varphi_j)]V_i^{2/3}+[1+u_j x_i(\varphi_j-\varphi_i)]V_j^{2/3}} \tag{6}$$

$$f_{ij}=\frac{2pV_i^{2/3}V_j^{2/3}\{p/q[(n_{ws}^{1/3})_i-((n_{ws}^{1/3})_j)]^2-(\varphi_i-\varphi_j)^2-b(r/p)\}\alpha_{ij}}{(n_{ws}^{1/3})_i^{-1}+(n_{ws}^{1/3})_j^{-1}} \tag{7}$$

$$\alpha_{ij}=1-0.1\times T[(1/T_{m_i})+(1/T_{m_j})] \tag{8}$$

The molar fractions of components i and j are expressed as x_i and x_j, respectively; the molar volume is V, the electro negativity is φ, the electron density is n_{ws}; α is the empirical constant; u, p, q and r are all empirical constants from Miedema model. Where p/q=9.4. b is the constant of 0.73 for liquid alloys and1.0 for solid alloys, respectively. In the miedema model, u=0.04 for the other metallic elements, u=0.07 for the trivalent metallic elements, and u=0.14 for the divalent metallic elements. p=10.6 when i and j are nontransition elements, p=12.3 when i and j belong to transition and nontransition elements, and p=14.1 when i and j are transition elements; the value of r/p is 0 if i and j are both nontransition or transition elements.

In a binary system, the relation of $\overline{G_i}^E$, G_{ij}^E, ΔH_{ij}, and S_{ij}^E are given as [14]:

$$\overline{G_i}^E = G_{ij}^E + (1+x_i)\frac{\partial G_{ij}^E}{\partial c_i} \tag{9}$$

$$G_{ij}^E = \Delta H_{ij} - TS_{ij}^E \tag{10}$$

With a certain temperature, the relationship between the interaction coefficient and the partial molar free energy can be shown as follows:

$$\varepsilon_i = \frac{1}{RT}\left(\frac{\partial \overline{G_i}^E}{\partial x_i}\right) \tag{11}$$

$$\varepsilon_i = \frac{1}{RT} f_{ij}\{[(4u_i+2u_j)(\varphi_j-\varphi_i)-2-2u_i u_j(\varphi_j-\varphi_i)^2/V_j^{2/3} -2[1+u_i(\varphi_i-\varphi_j)]\times[V_i^{2/3}(1+u_i(\varphi_i-\varphi_j))]+V_j^{2/3}(-1+u_j(\varphi_j-\varphi_i)]/(V_j^{2/3})^2\} \tag{12}$$

3.4 Extended Miedema model

In the $i-j-k$ ternary system, partial molar free energy can be calculated as:

$$\overline{G_i}^E = G^E - x_j\frac{\partial G^E}{\partial x_j} + (1-x_i)\frac{\partial G^E}{\partial x_i} \tag{13}$$

$$\overline{G_j}^E = G^E - x_i\frac{\partial G^E}{\partial x_i} + (1-x_j)\frac{\partial G^E}{\partial x_j} \tag{14}$$

$$\overline{G_k}^E = G^E - x_i\frac{\partial G^E}{\partial x_i} - x_j\frac{\partial G^E}{\partial x_j} \tag{15}$$

The Miedema model and the Toop model can

calculate the formation energy for the ternary alloy systems [15].

$$G^E = \frac{x_j}{1-x_i} G_{ij}^E(x_i, 1-x_i) + \frac{1-x_i-x_j}{1-x_i} G_{ik}^E(x_i, 1-x_i) + (1-x_i)^2 G_{jk}^E\left(\frac{x_j}{1-x_i}, \frac{1-x_i-x_j}{1-x_i}\right) \quad (16)$$

The relationship between the thermodynamic factor and the liquid-phase diffusion coefficient are given as follows:

$$D_i = \frac{x_i D_i^*}{RT} \frac{\partial u_i}{\partial x_i} = D_i^* g_i \quad (17)$$

When i is extremely dilute solute, D_i^* is the self-diffusion coefficient.

$$D_i = D_i^*(1+\varepsilon_i x_i) \quad (18)$$

$$D_j = D_j^*(1+\varepsilon_j x_j) \quad (19)$$

4. Results and discussion

Before calculating the activity coefficient and the liquid-phase diffusion coefficient, it was importance to consider the interaction coefficient in the solution. In the microstructure simulation, interaction among the alloy composition affected the course of nucleation and grains growth.

In order to verify the feasibility of the model, the liquid-phase diffusion coefficients of the Al-Ni[16-17], $AlFe_7$[18] and $Al_{87}Ni_{10}Ce_3$[19] melt that measured with experiment were calculated using the Extended Miedema model and Eyring model, respectively. The contrasts were shown in Table 2.

Table. 2. The contrast between the experimental diffusion coefficients (D^{Exp}) and the calculated ones (D^{Cal}).

Alloy	K	D^{Exp}	D^{Cal}
$AlNi_{10}$	1525	3.98×10^{-9}[16]	2.95×10^{-9}
$AlNi_{10}$	1795	5.2×10^{-9}[16]	4.01×10^{-9}
$AlNi_{20}$	1280	3.16×10^{-9}[17]	3.32×10^{-9}
$AlFe_7$	1053	3.98×10^{-10}[18]	2.1×10^{-10}
$Al_{87}Ni_{10}Ce_3$	1273	$(7.0\pm4.9)\times10^{-9}$(D_{Ce-Al}^{Exp}) [19]	3.7×10^{-9}(D_{Ce-Al}^{Cal})

In Table 2, the calculated results were similar to experimental results. Deviation of results was caused by two reasons. On one hand, the Extended Miedema model and Eyring model were adopted approximation in complex calculations. The errors were caused by the constant u , p , q and r in the Miedema model; the viscosity of Eyring model was provided by ProCAST, not given by the experiment. On the other hand, the error was caused by the experimental conditions. The estimated uncertainty of diffusion coefficient was about ±70% according to Garandet et al [20]. The measurement errors of diffusion coefficient were because of a similar capillary technique, namely the shear cell technique. The error estimation includes the measurement errors of position, length expansion coefficients, fitting error, effective diffusion time, temperature and concentrations.

The interact coefficient (ε) was calculated for the diffusion coefficient in Extended Miedema model with formulae 18 and 19. With the Extended Miedema model, the interaction coefficient curves were shown in Fig. 3. The interaction coefficient was decreased with the increasing temperature.

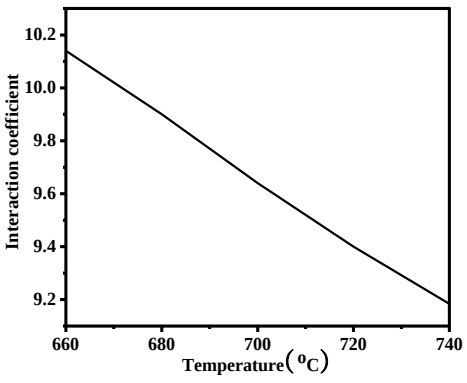

(a)

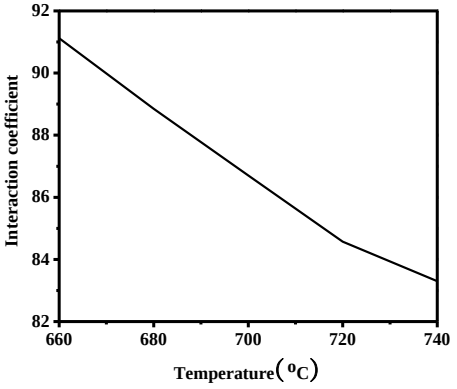

(b)

Fig. 3. Variation of alloy interaction coefficient with temperature during heating (a) Al-2%Cu alloy (b) Al-9.75Si-2%Cu alloy.

After calculating the interaction coefficient with temperature, the self-diffusion coefficient and liquid –phase diffusion coefficient were calculated by the Eyring model and the Extended Miedema model, respectively.

The black curve was the self-diffusion coefficient of different temperature in Fig. 4. As the Eyring model did not take the interaction of the alloy composition into account in the calculation process, the diffusion coefficient of Eyring model was the self-diffusion coefficient, and should be taken into the Miedema model to modify the data. The modified diffusion coefficient was shown with red line in Fig. 4.

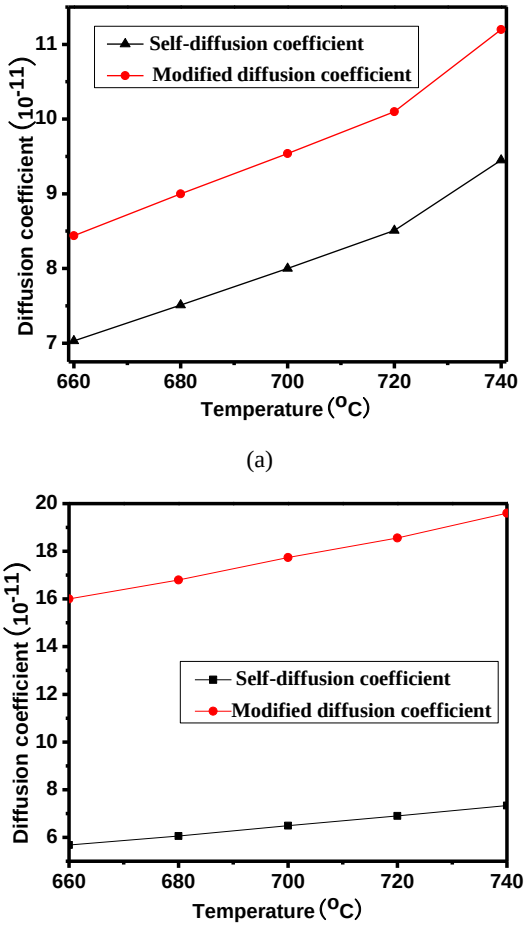

Fig. 4. Variation of alloy self-diffusion coefficient and modified diffusion coefficient with temperature during heating (a) Al-2%Cu alloy (b) Al-9.75Si-2%Cu alloy.

Before simulating the microstructure, the accurate temperature field must be acquired. The interfacial heat transfer coefficient (IHTC) was one of the most important parameters in temperature field simulation. The interfacial heat transfer coefficient was calculated according inverse identification of Zhang [21], the IHTC of casting-metal mold was identified by using the inverse analysis based on measured temperatures, neural network with back-propagation algorithm and numerical simulation. Temperature at various locations in the casting and mold was simulated by using the identified IHTC, and compared with the experimental measurement, to verify the feasibility of the method for determination of the casting-mold IHTC.

In numerical simulation, firstly, the inverse identified IHTC was taken into macroscopic temperature field to simulate temperature field accurately. Then, the microstructure simulation was further optimized by the modified diffusion coefficient of the melt. The microstructure was predicted with the finite elements and the cellular automata method.

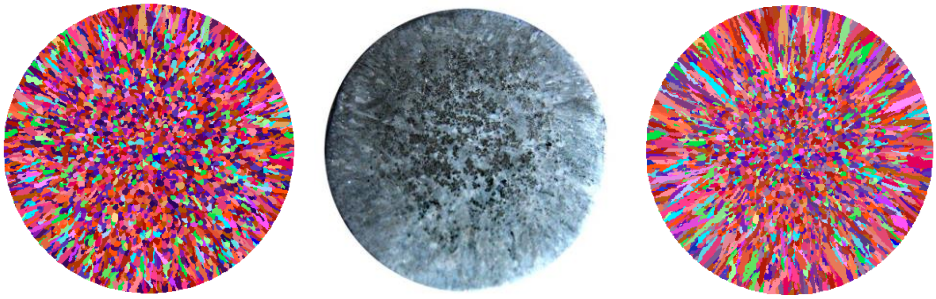

(a) (b) (c)

Fig. 5. Solidification structures of Al-2%Cu in the 40 mm casting (a) Simulation with the diffusion coefficient constant of 10^{-9} m^2/s, (b) Experimental microstructure (c) Simulation with the modified diffusion coefficient.

Table. 3 Statistical simulated results of Al-2%Cu in the 40 mm casting.

Statistical object	Columnar mean size (*m*)	Equiaxed mean size (*m*)	Proportion of columnar grains (%)
Simulation with 10^{-9} m^2/s	2.86×10^{-4}	13.3×10^{-5}	20.1
Experimental microstructure	3.05×10^{-4}	4.62×10^{-5}	58.1
Simulation with modified diffusion coefficient	3.67×10^{-4}	6.19×10^{-5}	64.8

In Fig. 5 and Table 3, the columnar to equiaxial transition was shown by the diffusion coefficient constant of 10^{-9} m^2/s, but the grain size was more different from experiment result. Especially, in the equiaxed grains size and proportion of columnar grains, the equiaxed grains size with diffusion coefficient constant of 10^{-9} m^2/s was 13.3×10^{-5}m, larger than the experimental equiaxed grains size of 4.62×10^{-5}m and the equiaxed grains size of 6.19×10^{-5} m with the modified diffusion coefficient. In proportion of columnar grains, the results with the modified diffusion coefficient were 64.8% and closer to the experimental results of 58.1%, but the results used the diffusion coefficient constant was just 20.1%. It could be seen that the simulation with the modified diffusion coefficient could veraciously reflect the grain distribution in Fig. 5c.

(a) (b) (c)

Fig. 6. Solidification structures of Al-9.75Si-2%Cu in the 40mm casting (a) Simulation with diffusion coefficient constant of 10^{-9} m^2/s (b)Experimental microstructure (c) Simulation with the revised diffusion coefficient curve.

Table 4. Statistical simulated results of Al-9.75Si-2%Cu in the 40 mm casting.

Statistical object	Equiaxed mean size (*m*)
Simulation with 10^{-9} m^2/s	1.26×10^{-3}
Experimental microstructure	2.11×10^{-3}
Simulation with modified diffusion coefficient	1.63×10^{-3}

In Fig. 6 and Table 4, the simulation results with modified diffusion coefficient were similar to the ones with diffusion coefficient constant of $10^{-9}m^2/s$, because the diffusion coefficient of the Al-9.75Si-2%Cu melt was ranged from 1.61×10^{-9} m^2/s to 1.96×10^{-9} m^2/s. It was a little difference with the diffusion coefficient constant of 1.0×10^{-9} m^2/s. In Table 4, the equiaxed mean size with modified diffusion coefficient was more similar to the experimental size than the equiaxed grains mean size with diffusion coefficient constant of 10^{-9} m^2/s.

5. Conclusions

As the diffusion coefficient of a melt was usually assumed to a constant of 1×10^{-9} m^2/s in various numerical simulations, the diffusion coefficients of Al-2%Cu melt and Al-9.75Si-2%Cu melt were calculated by the Miedema model, Extended Miedema model and Eyring model in different temperatures, respectively.

Comparing the simulation results, the results with the modified diffusion coefficient was more accurate than the results with the diffusion coefficient constant in equiaxed grains size and the proportion of columnar grains. With the modified diffusion coefficient, the results could reflect the grain distribution, size of equiaxed and columnar grains accurately. The calculation model of the diffusion coefficient could compensate for the lack of experimental data in the liquid diffusivity.

Acknowledgement

The authors gratefully acknowledge research support from the National Natural Science Foundation of China (No.51075132), The Doctoral Fund of Ministry of Education of China (No.20090161110027).

References

[1] M. Rappaz, Int. Mater. Rev. **34**, 93 (1989).
[2] C. Y. Wang, C. Beeckrmann, Metall. Mater. Trans. **27A**, 2754 (1996).
[3] Ch. A. Gandin, M. Rappaz, Acta. Metall. Mater. **42**, 2233 (1994).
[4] H. Takatani, Ch. A. Gandin, M. Rappaz, Acta. Mater. **48**, 675 (2000).
[5] A. Takeuchi, A. Inoue, Intermetallics. **18**, 1779 (2010).
[6] S. P. Sun, D. Q. Yi, H. Q. Liu, B. Zang, Y. Jiang, J All Com. **506**, 377 (2010).
[7] P. K. Ray, M. Akinc, M. J. Kramer, J All Com. **489**, 357 (2010).
[8] S. P. Sun, D. Q. Yi, Y. Jiang, B. Zang, C. H. Xu, Y. Li, Chem. Phys. Lett. **513**, 149 (2011).
[9] Z. W. Chen, C. Y. Ma, P. Chen, Trans. Nonferrous. Met. Soc. China. **22**, 42 (2012).
[10] X. H. Yan, W. H. Tang, Z. Y. Qiao, G. H. Rao, J. K. Liang, S. S. Xie, J. Rare. Earths. **4**, 252 (1993).
[11] X. Y. Ding, P. Fan, Q. Y. Han, Acta.Metall. **30**, 50 (1994).
[12] S. Glasstone, K. J. Laidler, H. Eyring, The Theory of Rate Process, McGraw, NY, 1941.
[13] M. Kuriyagawa, T. Kawamura, S. Hayashi, K. H. Nitta, J. Mater. Sci. **46**, 1264 (2011).
[14] X. Q. Chen, X. Y. Ding, X. LIU, H. Y. Zheng, Acta. Metall.sin. **36**, 492 (2000).
[15] G. W. Toop, Trans. Metall. Soc. AIME. **233**, 850 (1965).
[16] S. K. Das, J. Horbach, M. M. Koza, S. M. Chatoth, A. Meyer, Appl. Phys. Lett. **86**, 011918 (2005).
[17] J. Horbach, S. K. Das, A. Griesche, M. P. Macht, G. Grohberg, A. Meyer, Phys. Rev. B. **75**, 174304 (2007).
[18] L. J. Zhang, Y. Du, Lngo. Steinbach, Q. Chen, B. Y. Huang, Acta. Mater. **58**, 3664 (2010).
[19] A. Griesche, M. P. Macht, G. Frohberg. Acta. Mater. **353**, 3305 (2007).
[20] J. P. Garandet, G. Mathiak,V. Botton, P. Lehmann, A. Griesche, Int. J. Thermophys. **25**, 249 (2004).
[21] L. Q. Zhang, L. X. Li, H. Ju, B. W. Zhu. Energ. Convers. Manage. **51**, 1898 (2010).

*Corresponding author: llxly2000@163.com